JOURNAL OF BACTERIOLOGY, Nov. 1987, p. 5008–5015
0021-9193/87/115008-08$02.00/0

Vol. 169, No. 11

Three-Dimensional Structure of the Regular Tetragonal Surface Layer of *Azotobacter vinelandii*

WADE H. BINGLE,[1]† HARALD ENGELHARDT,[2] WILLIAM J. PAGE,[1]* AND WOLFGANG BAUMEISTER[2]

Department of Microbiology, University of Alberta, Edmonton, Alberta, Canada T6G 2E9,[1] and Max-Planck-Institut für Biochemie, D-8033 Martinsried, Federal Republic of Germany[2]

Received 4 June 1987/Accepted 17 August 1987

Fragments of the *Azotobacter vinelandii* tetragonal surface (S) layer, free of outer membrane material, were obtained by treating whole cells with 100 μM EDTA. The three-dimensional structure of the S layer was reconstructed from tilted-view electron micrographs of the S-layer fragments, after computer-assisted image processing by correlation averaging. At a resolution of 1.7 nm, the S layer exhibited funnel-shaped subunits situated at one fourfold-symmetry axis and interconnected at the other fourfold-symmetry axis to form prominent cruciform linking structures. These data, in conjunction with a relief reconstruction of the surface of freeze-etched whole cells, indicated that the apex of the funnel-shaped subunit was associated with the outer membrane, while the funnel "opening" faced the environment; the cruciform linking structures were formed at the outermost surface of the S layer. Electron microscopy and image enhancement were used to compare the structure of the outer membrane-associated S layer with that of fragments of the S layer dislodged from the outer membrane. This analysis revealed an increase in the lattice constant of the S layer from 12.5 to 13.6 nm and an alteration in the position of the cruciform linking structures in the *z* direction. These conformational changes resulted in a reduction in the thickness of the S layer (minimum estimate, 5 nm) and an apparent increase in the size of the gaps between the subunits. In terms of the porosity of the S layer, this gave the appearance of a transition from a closed to a more open structure.

Despite the first identification of regularly arranged protein subunits on the surface of a *Spirillum* species over 30 years ago (21) and subsequent investigations which showed that these structures are common components of procaryotic cell walls, surface (S) layers have received relatively little attention. This is probably because neither *Escherichia coli* nor *Bacillus subtilis* possesses an S layer, and these structures can be difficult to demonstrate by using commonly used electron microscopic preparative techniques such as negative staining and freeze-etching (22, 29).

Azotobacter vinelandii is an obligately aerobic, nitrogen-fixing, soil bacterium closely related to the fluorescent pseudomonads, members of the gamma subdivision of the purple photosynthetic gram-negative eubacteria (11, 30). The subject of numerous electron microscopic studies during the past 20 years, this organism was only recently shown to possess a regular S layer of tetragonal organization external to the outer membrane (5). The difficulty experienced in detecting the S layer of *A. vinelandii* may be a situation common to other eubacteria. Although finally discovered by freeze-etching, *A. vinelandii* cells require a pretreatment thought to remove overlying capsular material which may collapse over the S layer during etching. Additionally, negative staining of this S layer is only successful with ammonium molybdate because the array is disrupted by other commonly used negative stains such as uranyl acetate and phosphotungstic acid (7).

The relatively recent ability to negatively stain the *A. vinelandii* S layer has allowed the application of conventional Fourier-based image enhancement methods for the determination of its projection (two-dimensional; 2-D) structure (7). Although the resolution obtained was relatively low (4 nm), the structure was shown to be quite similar to a particular conformation of the tetragonal S layer present on the phylogenetically related bacterium *Aeromonas salmonicida* (31). However, it has become clear that apparent similarities between 2-D structures may not extend to the level of a three-dimensional (3-D) structure (12, 15). Thus, any meaningful structural comparisons between S layers require full 3-D structures. We report here the 3-D structure of the *A. vinelandii* S layer obtained by using a reconstruction scheme which involves the use of "correlation averaging," an image-processing technique which, unlike conventional Fourier-based methods, partially compensates for lattice distortions (26). In addition, fragments of the S layer free of underlying outer membrane material were obtained for the first time. These two improvements partly contributed to the determination of the 3-D structure of the *A. vinelandii* S layer to a resolution of 1.7 nm; at this resolution, new details of the structure emerged. We also noted an increase in the lattice constant of the *A. vinelandii* S layer upon dissociation from the outer membrane, and an apparent increase in S-layer porosity. A similar observation was reported for the S layer of *A. salmonicida* (31); the significance of these observations is discussed.

MATERIALS AND METHODS

Bacterial strain, S-layer preparation, and negative staining. *A. vinelandii* OP strain UW1 (capsule$^-$) was grown for 12 h with vigorous aeration in Burk medium (7) to a final optical density at 620 nm of between 0.8 and 1. The cells were washed in 5 mM potassium phosphate buffer, pH 7.2, to remove excess divalent cations. S-layer fragments free of underlying outer membrane were obtained by suspending

* Corresponding author.
† Present address: Department of Microbiology, University of British Columbia, Vancouver, British Columbia, Canada V6T 1W5.

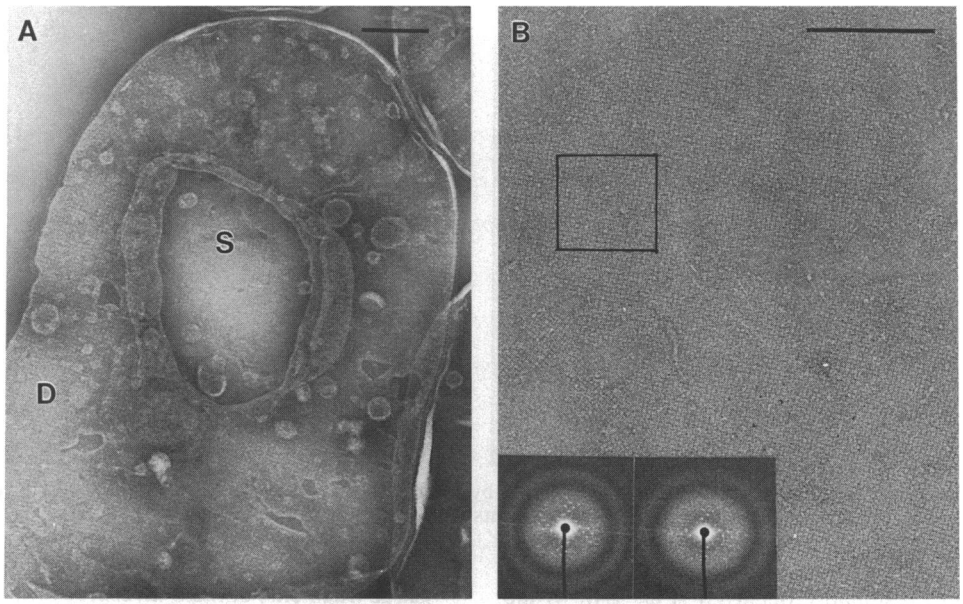

FIG. 1. Electron micrographs of the S layer of *A. vinelandii* negatively stained with ammonium molybdate. (A) S layer associated with the cell wall showing double (D)- and single (S)-layered areas. (B) S layer fragment dislodged from the cell wall. The boxed area of this fragment containing 470 unit cells was used for the 3-D reconstruction; the inset shows light optical diffractograms obtained of the fragment at the beginning (left) and end (right) of the tilt series. Bars, 200 nm.

these cells to an optical density of 20 in 100 mM Tris hydrochloride–100 μM EDTA, pH 8, which caused large fragments of the S layer to be dislodged from the cell surface. Samples of the cell suspension in Tris-EDTA buffer were applied directly to glow-discharged carbon-coated copper grids and stained with 4% ammonium molybdate in Burk buffer (7); the stain was adjusted to pH 6 with ammonium hydroxide before use.

The S layer in its native state, i.e., attached to the outer membrane, was visualized through negative staining by preparing *A. vinelandii* "ghosts" by a modification of the method of Robish and Marr (24); this method involved subjecting whole cells to plasmolysis with 5 M glycerol followed by osmotic shock. The cytoplasmic membrane of the resulting large particles (see reference 24 for terminology) was solubilized with 1% Triton X-100. Except for the Triton X-100 treatment, in which 5 mM potassium phosphate buffer was used, Burk buffer was used throughout as the diluent so as to ensure the proper ionic environment for the integrity of the array. The ghosts were suspended in Burk buffer containing 1% glutaraldehyde and stained with 2% ammonium molybdate as described above.

Electron microscopy and image processing. Electron micrographs were made at a magnification of 36,000×, using a Philips EM 420 electron microscope equipped with an unlimited-tilt specimen holder (9). Tilt series were recorded by following a scheme outlined by Saxton et al. (27), and all micrographs were examined by using an optical diffractometer to ensure appropriate focus and minimum astigmatism. Regions of the negatives containing S-layer fragments exhibiting satisfactory crystallinity and satisfying the above criteria were digitized by densitometry in a matrix of 512^2 pixels with a step size of 20 μm; this corresponds to a translation of 0.56 nm at the specimen level. Finally, all images were subjected to correlation averaging (26) to define the average unit cell.

3-D and surface relief reconstructions. The 3-D reconstruction was performed by using substantially conventional methods (1) as outlined in detail by Saxton et al. (27) and Baumeister et al. (2). The sidedness of the S layer was determined by performing a surface relief reconstruction of unidirectionally platinum-carbon-shadowed, freeze-etched whole cells. Freeze-etch replicas were made as outlined previously (5), and micrographs were taken and digitized as described above. Images of freeze-etched cells were subjected to correlation averaging, and then one of them was subjected to correspondence analysis (16) to obtain selective, i.e., more homogeneous, averages from the somewhat curved and undulated cell surface. Correspondence analysis was performed according to a variant described previously (14), using 480 unit cells extracted from the source image. The images were classified with respect to the first four eigenvectors, using the intra- and interclass distances as sorting criteria (R. Hegerl, unpublished data). Four classes were defined, and the corresponding unit cells were selectively averaged; the classification criterion proved to be the variability of the platinum deposition on the surface due to different inclinations of the morphological complexes with respect to the metal beam. Surface relief reconstruction was performed as described by Guckenberger (18) and Baumeister et al. (4), starting with the selectively averaged unit cells.

Both the 3-D model and the surface relief reconstruction were visualized by using a surface-shading program which essentially produces simulated photographs of the S layer as if it possessed a reflective surface and was illuminated from the right at an angle of 45° (25).

RESULTS

Projection structure of the S layer. Preparation of *A. vinelandii* ghosts yielded large particles retaining the shape of the cell possessing one large, centrally located hole where

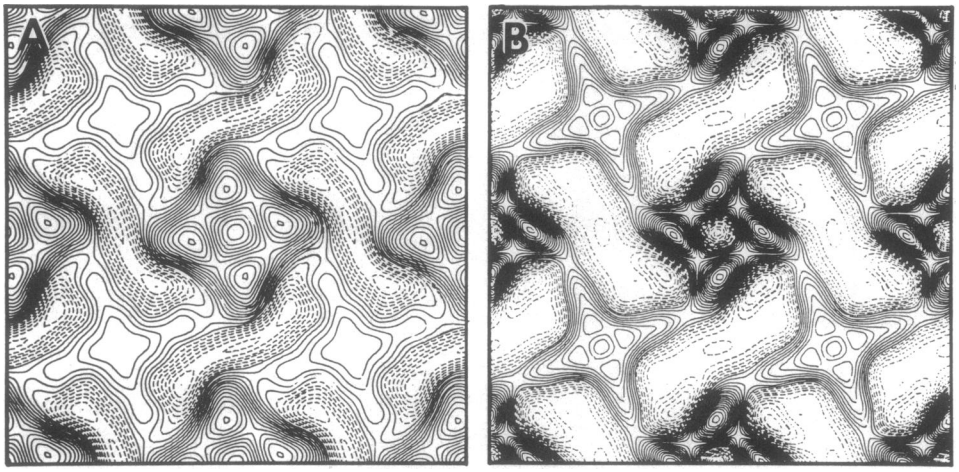

FIG. 2. Projection structures of the *A. vinelandii* S layer obtained by correlation averaging of a number of electron micrographs containing areas of (A) the cell wall-associated S layer and (B) S-layer fragments dislodged from the cell wall.

osmotic disruption presumably occurred (Fig. 1A). While the tetragonal S layer was clearly visible, covering the entire ghost, optical diffractograms indicated that these areas were composed of superimposed lattices and that the separation of the lattices for correlation averaging, while possible (20), would be a formidable task in this case. Therefore, single-layered areas of the S layer visible through the holes in the cell wall were averaged (Fig. 1A). Correlation averaging of a number of such holes produced in projection, at a resolution of 2 to 2.5 nm, a pattern of two alternating, interconnected tetrameric subunits (Fig. 2A). The lattice constant based on three determinations was $a = b = 12.5 \pm 0.3$ nm.

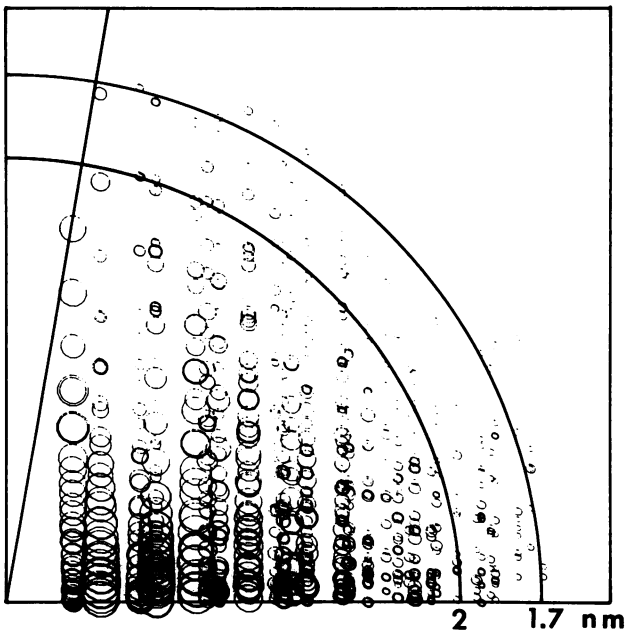

FIG. 3. Distribution of data in Fourier space. The ordinate corresponds to the z^* axis and the abscissa to the r^* axis ($r^{*2} = x^{*2} + y^{*2}$), respectively. The area of each circle is proportional to the modulus of the corresponding Fourier coefficient. The curves indicate resolution spheres at 2 and 1.7 nm and the line the "missing cone" left by tilting to 80.6°.

Large fragments of the S layer free of the outer membrane were obtained by exposing whole cells to a low concentration of EDTA (100 μM) in 100 mM Tris hydrochloride, pH 8 (Fig. 1B). The objective of this treatment was to chelate the divalent cations partly responsible for the attachment of the S layer to the outer membrane (5); the high concentration of Tris was to maintain the ionic strength and to disrupt the outer membrane through its dispersive effect on lipopolysaccharides. Correlation averaging of the structure present in the S-layer fragments dislodged from the outer membrane produced a projection structure (resolution of 1.7 nm according to the radial correlation function criterion [26]) with the same features as those of the average of the membrane-associated array (Fig. 2B). However, the lattice constant was significantly increased by 1.1 nm to 13.6 ± 0.1 nm (5 determinations), which was associated with a clockwise rotation of the central tetrameric subunit by about 16° as compared with that of the membrane-associated layer. Assuming that the stain-filled areas are gaps in the S layer, in terms of porosity, a transition from a closed to a more open structure was evident.

Assessment of data used for 3-D reconstruction. Although it may have been preferable to reconstruct the 3-D structure of the membrane-associated S layer, the determination of this structure was difficult because the holes in the ghosts were generally too small to record images at the very high tilt angles necessary for a reliable 3-D reconstruction. Attempts at preparing relatively unperturbed outer membrane-associated single S-layer sheets by controlled cell disruption in the French pressure cell were unsuccessful; double-layered membrane vesicles predominated even when disruption was carried out at 20,000 lb/in^2. Moreover, the averages obtained from membrane-associated S layers tended to have a somewhat lower resolution. We therefore decided to reconstruct the 3-D structure of the S layer from tilted views of negatively stained S-layer fragments free of the outer membrane support. Negative staining of S-layer fragments free of underlying outer membrane material generally produced images of low contrast (Fig. 1B). This necessitated searching for suitable S-layer fragments at high magnifications (30,000×) which could have resulted in some additional radiation damage. However, neither optical diffractograms nor the computed power spectra of the two nominal 0° tilt images, one recorded at the beginning of the tilt series and

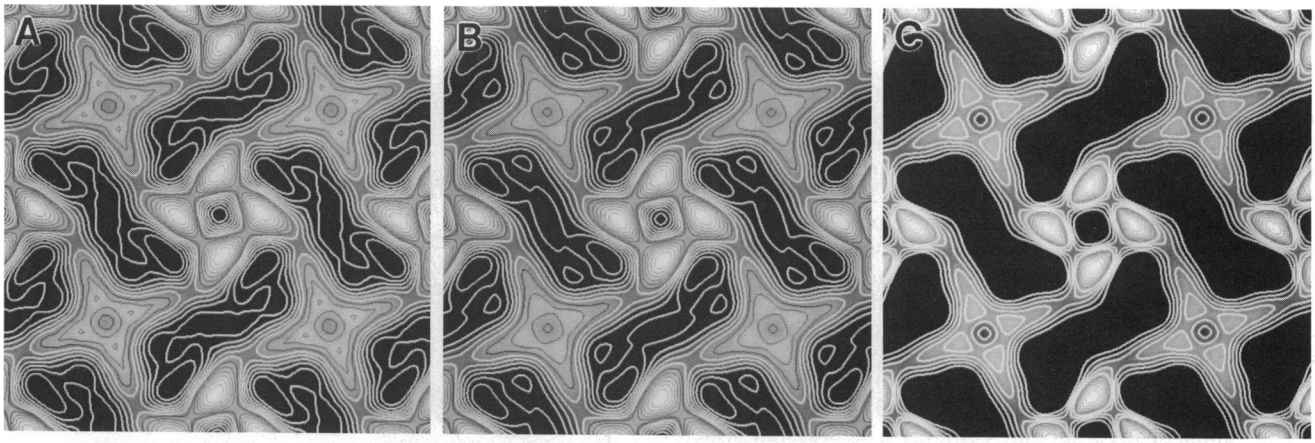

FIG. 4. Maps of the *A. vinelandii* S layer obtained from (A) an average of a 0° tilt micrograph used for the 3-D reconstruction, (B) an appropriate projection through the 3-D reconstruction, and (C) a corresponding projection through the 3-D reconstruction after thresholding as applied for calculating the models presented in Fig. 5. Dimensions of each image, 27 by 27 nm.

one recorded at end of the tilt series, showed any serious radiation damage (Fig. 1B, inset). As expected from the previous study (7), the optical diffractograms indicated a structure with p4 symmetry and unambiguous handedness. Nineteen projections with actual tilt angles between 0 and 80.6° were used for the 3-D reconstruction. The specimen inclination normal to the tilt axis was determined to be 4.3°. The distribution of data in Fourier space (Fig. 3) showed heavy filling to a resolution of 2 nm, with lighter filling to a resolution of 1.7 nm. Because tilt angles up to 80° were used, only the 1,0 lattice line was incompletely covered.

The consistency of the reconstruction with the original projections was judged by comparing averages of the tilted images with corresponding projections through the 3-D reconstruction, using the original data as well as the thresholded reconstruction applied for model building. The projections of the thresholded data were apparently identical to the original averages (Fig. 4), except for very faint density variations in the gaps which do not appear in the projected model consisting of almost 90% of the expected mass.

3-D structure of the *A. vinelandii* S layer. The 3-D model of the *A. vinelandii* S layer is presented in Fig. 5 as computer-generated views of the two surfaces of the S layer. These surface-shaded representations give the impression that the central tetrameric subunit of the projection structure (Fig. 2B) is funnel shaped and flattened at the apex. These subunits, situated at one fourfold-symmetry axis, are interconnected at the other fourfold-symmetry axis to form cruciform linking structures. Because freeze-etch replicas of whole cells exhibit subunits separated by a distance of 12.5 nm (7) to be consistent with the 3-D model (Fig. 5), these subunits must represent either the cruciform linking structures or the apex of the funnel-shaped subunits. A relief reconstruction of freeze-etched cells revealed tetrameric structures whose shape could not unambiguously identify which of the subunits was shadowed (Fig. 6). However, the orientation of the linking arms of the cruciform subunits allowed us to determine the sidedness of the S layer. The surface relief reconstruction is only compatible with the 3-D reconstruction, if we assume that the cruciform linking

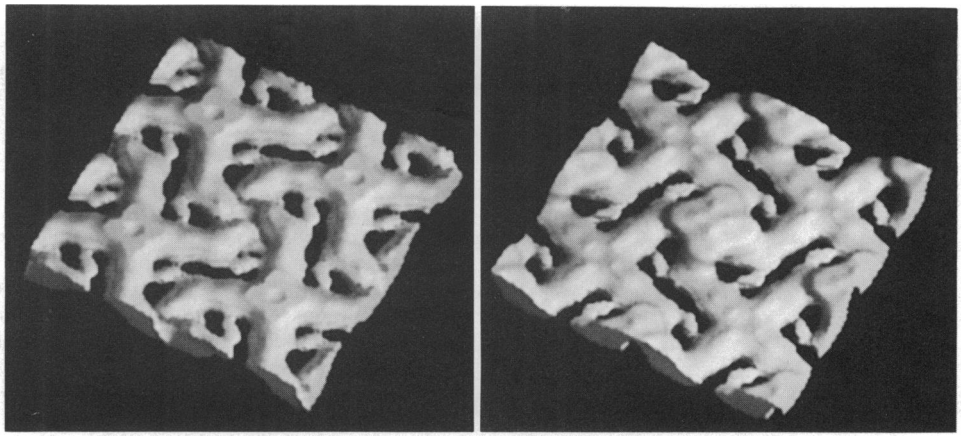

FIG. 5. Computer-generated views of the two surfaces of the 3-D reconstruction of the *A. vinelandii* S layer, using a surface-shading program. The funnel-shaped subunit is located in the center of the figure surrounded by the cruciform linking structures: (left) outer surface of the S layer (Fig. 6); (right) inner surface of the S layer. About 90% of the expected volume is included in the model. Dimensions of each image, 27 by 27 nm.

structures are situated at the outer layer surface. The apex of the funnel-shaped tetramer, therefore, is in contact with the underlying outer membrane.

The S layer shows a pronounced relief in the freeze-etched preparation (Fig. 6); i.e., the linking arms have a significant inclination with respect to the layer plane. However, the impression from Fig. 5 is that the outer surface of the S layer is quite flat; vertical sections through the 3-D reconstruction confirm this impression (Fig. 7). Therefore, the conformational changes of the layer dislodged from the cell surface appear also to alter the position of the linking arms in the z direction and to reduce, thereby, the thickness of the layer. In addition, some flattening of the isolated layer upon adsorption to the specimen support may occur. We conclude, therefore, that the lower limit of the thickness of the layer is about 5 nm, as suggested by the 3-D reconstruction.

The funnel-shaped subunit contains a depression which does not appear to open at the inner surface (Fig. 7). However, as has been pointed out before (15), this feature is difficult to discern because of possible artifacts caused by the flattening of the S layer against the carbon film (see above), especially if the pore diameter approaches the resolution limit. By analogy to other S layers, the region of funnel-shaped subunit near the outer membrane (or peptidoglycan in gram-positive organisms) can be referred to as a core domain (3). The structure of this domain is illustrated by examining horizontal sections (z slices) through the reconstruction (Fig. 8).

The gaps in the S layer are basically parallelograms in projection, arranged in a simple cobblestonelike pattern and apparently open down to the outer membrane (Fig. 2B and 7). Indeed, a 3-D model of the S layer, thresholded to consist of 73% of the expected mass (data not shown), using a protein density of 1.37 g/cm^3 and a molecular weight of 60,000 for the monomer (6), did not contain any structure in the gaps, suggesting that they are completely open with

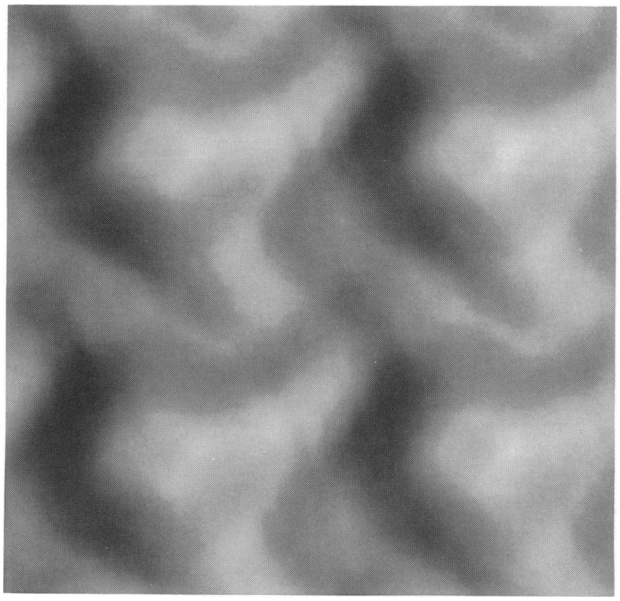

FIG. 6. Relief reconstruction of the outer surface of freeze-etched whole cells of *A. vinelandii* viewed at an angle of 90°. The center shows the funnel-shaped tetramer. Dimensions of the image, 27 by 27 nm.

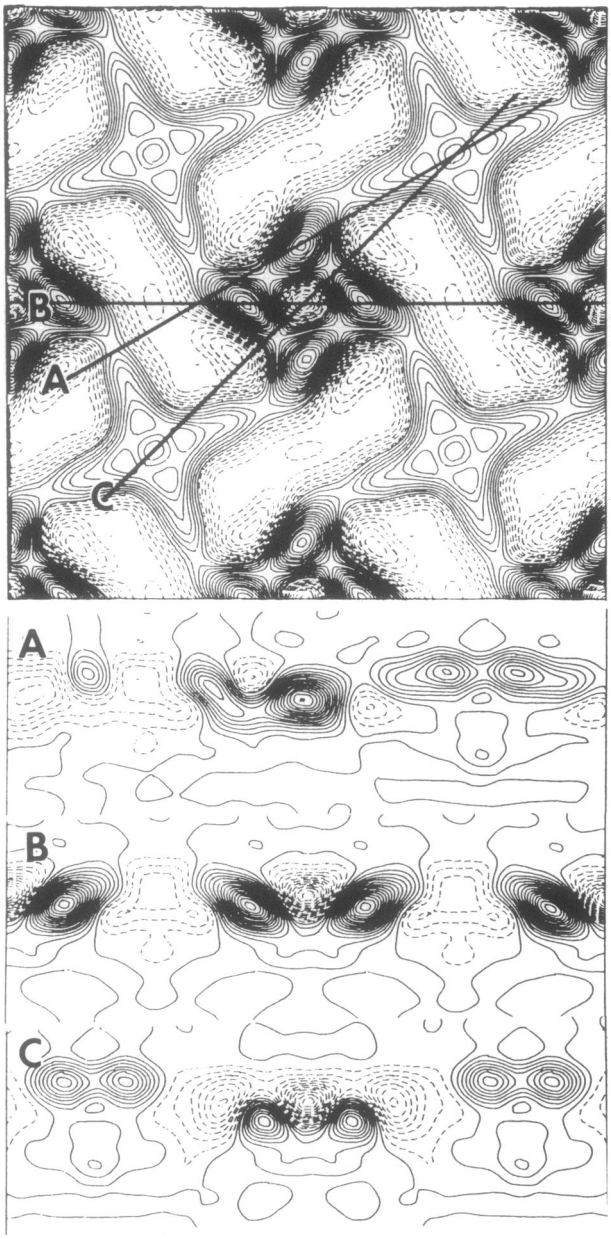

FIG. 7. Vertical sections through the 3-D reconstruction. The upper panel showing the 3-D reconstruction in projection indicates the position of the vertical sections. The sections are oriented so the outer surface of the S layer is at the top; the size of each section is 27 by 9.3 nm.

maximal dimensions of 11 by 3.5 nm. The averages of the (untilted) layer as well as the projection through the 3-D reconstruction, however, show some density variations within the gaps with additional stain accumulation close to the funnel-shaped tetramers (Fig. 4). Taking the contour levels as a relative measure for the approximate thickness, the features in the gaps account for ~1/6 of the total thickness of the layer, i.e., less than 1 nm. Such fine details may exist as local density variations in the 3-D reconstruction; of course, because of the limiting resolution, the exact size and shape cannot be obtained. If the 3-D model is forced to contain almost 90% of the expected volume (usually only

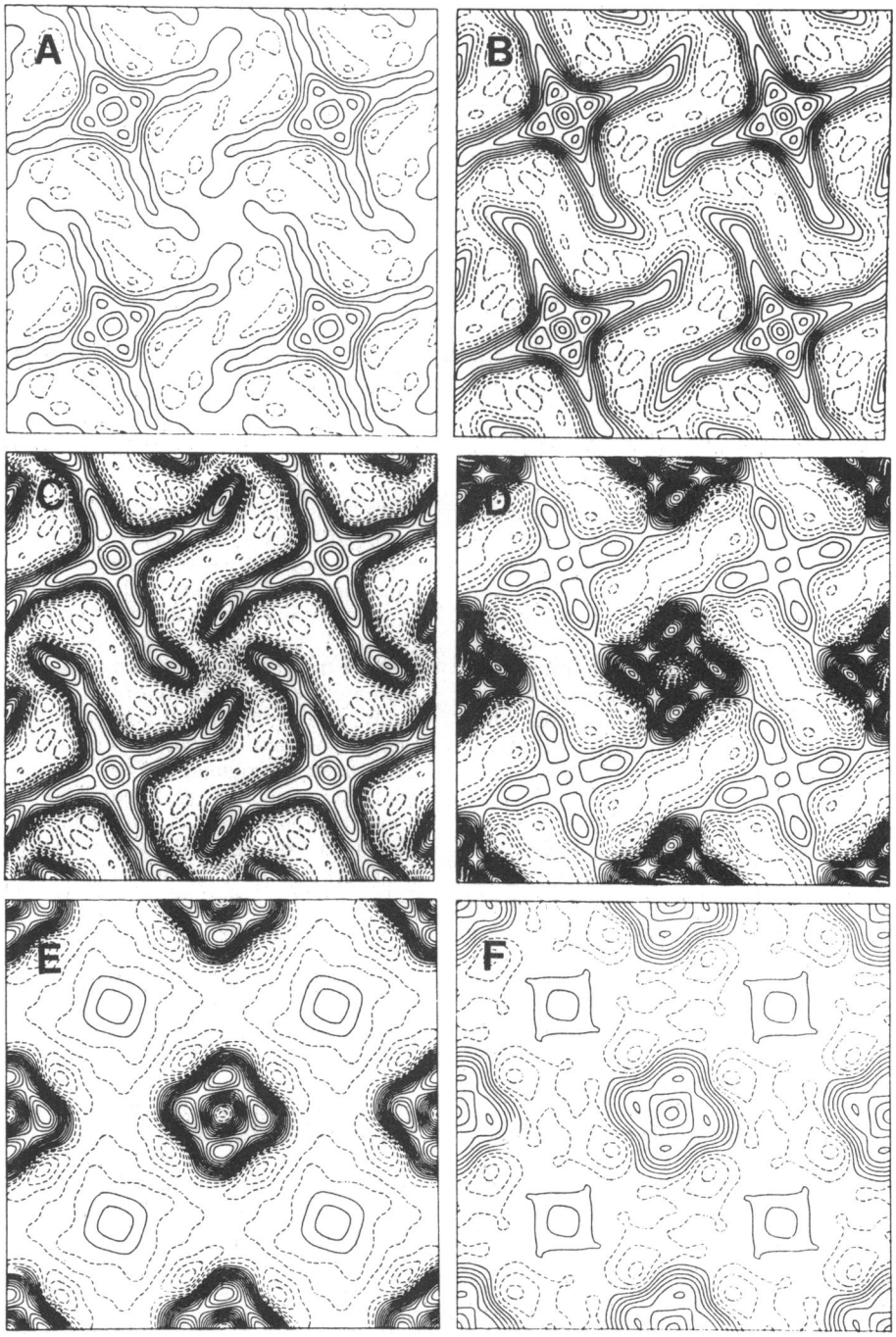

FIG. 8. Horizontal sections through the 3-D reconstruction beginning at the outer surface of the S layer and moving toward the inner surface. Sections A to C show the cruciform linking structures, and sections D to F show the core domain. The sections are separated by a distance of 0.6 to 0.75 nm.

50 to 75% of the volume is presented in 3-D models), small features (about 1 nm thick) near the central layers of the linking arms can be seen connecting the neighboring arms (Fig. 5). The gaps are narrower, and holes near the funnel-shaped tetramers are developed which could indeed contribute to the local stain accumulation found in the 2-D projections (Fig. 4). Probably the gaps are not completely open but contain small protein domains. The 3-D model in Fig. 5 indicates the position of the small features within the gaps but does not provide their correct size and shape with certainty.

DISCUSSION

A number of differences have emerged between the previously reported Fourier-based 2-D structure of the *A. vinelandii* S layer (7) and the 3-D reconstruction reported here, the most notable difference being the lattice constant of the S layer. Bingle et al. (7) reported a lattice constant of 18.4

nm for S-layer fragments partially associated with outer membrane material. This value has been rechecked and found to be the diagonal spacing of the subunits; the corresponding lattice constant is therefore 13.0 nm. This figure occupies an intermediate position between the lattice constants for the open and closed conformations of the S layer studied here.

The cruciform linking structures are much more prominent in the present reconstruction than would have been anticipated by examining the 2-D average presented by Bingle et al. (7), where the linkers of the array were very delicate and did not appear to constitute a significant portion of the protein mass. This observation led to the proposal that distilled water, which dissociates the S layer into tetrameric units, does so by disrupting the linking region and that the funnel-shaped subunit could be viewed as the building block of the array. This suggestion was supported by the observation that S-layer formation could only be observed in reassembly experiments if preformed tetramers were present (7, 13). However, based on the present model, it is equally likely that the cruciform linking structures represent the building blocks of the S layer. Recently, a striking structural analogy between the S layers of *A. vinelandii* and *Desulfurococcus mobilis* has been identified (I. Wildhaber and W. Baumeister, unpublished data); *D. mobilis* also possesses an S layer with p4 symmetry with prominent cruciform morphological units as building blocks. These S layers, while possessing a similar basic architecture, differ slightly; the *A. vinelandii* S layer is classified as an M_4C_4 type according to the scheme of Baumeister et al. (2), while the *D. mobilus* layer is an M_4C_2 type.

The previous 2-D average of the *A. vinelandii* S layer (7) also showed a striking similarity to the projection structure of a particular conformation of the *A. salmonicida* tetragonal S layer (31). Recently, the 3-D structure of this S layer has been completed (Engelhardt and Baumeister, manuscript in preparation). Like the *A. vinelandii* S layer, the *A. salmonicida* surface array is composed of funnel-shaped subunits located at one fourfold axis interlinked at the outer surface of the S layer via the other fourfold axis. While the core domains of these S layers appear quite similar, the interconnecting domains are quite dissimilar. The *A. salmonicida* array has only a minor portion of the protein mass involved in the linking region, confirming the impression given by the 2-D average (31). Thus, while the *A. salmonicida* S layer appears to exhibit weaker connectivity than the *A. vinelandii* array, it does not exhibit the peculiar "aqualability" exhibited by the *A. vinelandii* S layer. These comparisons indicate that it is probably hazardous to try to correlate the resistance of some S layers to dissociation by chemical perturbants with the apparent extent of connectivity of their linking regions (see also reference 10).

Compared with the tetragonal S layers of *Bacillus sphaericus* P-1 (23) and *Sporosarcina ureae* (15), the mass distribution in the *A. vinelandii* tetragonal S layer is relatively simple. The S layers of these gram-positive bacteria show multiple protein domains of different masses arranged in three planes in the z direction leading to a complex distribution of pores and gaps of differing sizes. The *S. ureae* and *B. sphaericus* layers are built from proteins of 115,000 and 140,000 molecular weight, respectively, while the *A. vinelandii* S layer is composed of a protein of only 60,000 molecular weight. Therefore, the former proteins could obviously accommodate a more complex domain structure. Such differences might have been expected from the differences in molecular weight between the proteins which constitute each layer, as well as their projection structures, but the different complexities of these S layers are only clearly appreciated by examining their 3-D structures. Not only do the core regions appear almost identical between the S layers of *A. vinelandii* and *A. salmonicida*, but a comparison to the corresponding domains of the S layers of the phylogenetically unrelated bacteria *S. ureae* and *B. sphaericus* S layers also reveals striking similarities. This observation and those of Engelhardt et al. (15) confirm similar observations made for the hexagonal S layers carried by a number of phylogenetically unrelated bacteria (3); i.e., the tetragonal S layers of both gram-positive and gram-negative bacteria appear to exhibit a conserved core structure and show most of their diversity at the outer surface and in the linking region.

In the present study, a small but significant alteration in the structure of the S layer was noted upon removal from the cell wall. This was characterized by a rotation of the funnel-shaped subunit, an increase in the lattice constant, and a transition, in terms of porosity, from a closed to a more open structure. An increase in the lattice constant and S-layer porosity was reported for the S layer of *A. salmonicida* by Stewart et al. (31), but the apparent increase in porosity was much more pronounced than that observed for the *A. vinelandii* S layer. Stewart et al. (31) speculated that the transition to the open conformation could be used to increase the permeability of the S layer. Unlike the present study, where the closed conformation was exclusively cell wall associated and the open conformation was present exclusively in fragments of the S layer released from the cell wall, Stewart et al. (31) found both the open and closed conformations of the *A. salmonicida* S layer in fragments dislodged from the cell surface. Second, no averages were available for the outer membrane-associated S layer of *A. salmonicida* to discern whether both conformations were also present on the cell surface in vivo. In fact, subsequent studies revealed only the type I (closed) conformation of the S layer both on and off the cell surface (Engelhardt and Baumeister, manuscript in preparation). These observations support the idea that the transition to the open conformation may be a consequence of the release of the S layer from the cell wall with no functional significance in vivo and that the production of the type II (open) conformation could be due to preparation differences between laboratories. Certainly, as pointed out by Stewart et al. (31), conditions must be identified which reliably produce the type II conformation of the *A. salmonicida* S layer to resolve these important outstanding questions.

It has usually been inferred that isolated S layers or those formed as a consequence of reassembly in vitro possess structural properties similar to those of native arrays attached to the cell wall because both exhibit the same general appearance when examined by negative staining. However, even early experiments showed that the two structures can be different because isolated or reassembled S layers are more easily disrupted than native arrays anchored to the cell wall (8, 17, 19, 28). In fact, recent experiments with S-layer reassembly in *A. vinelandii* (13) show that reassembled layers do not necessarily return to the native state and that an association with the outer membrane that is achieved in vivo but not in vitro is important to S-layer stability. This observation that the association with the underlying outer membrane is important to the stability of the S-layer complements the observations reported here that detachment of the S layer from the cell surface may produce a subtle and perhaps inevitable alteration in its structure. These observa-

tions provide a warning that the association of the underlying cell wall may be important to the dimensions of the S-layer structure and to its integrity. Resolution of the conformational changes is likely to require sophisticated microscopy and image analysis.

ACKNOWLEDGMENTS

We thank U. Santarius for excellent technical assistance and J. L. Doran for assistance with the preparation of the freeze-etch replicas.

This work could not have been conducted without financial assistance of the Max-Planck-Institut für Biochemie provided to W.H.B. in Martinsried, Federal Republic of Germany. Partial support was obtained from the Natural Sciences and Engineering Research Council of Canada in the form of an operating grant to W.J.P.

LITERATURE CITED

1. **Amos, L. A., R. Henderson, and P. N. T. Unwin.** 1982. Three-dimensional structure determination by electron microscopy of two-dimensional crystals. Prog. Biophys. Mol. Biol. **39**:183–231.
2. **Baumeister, W., M. Barth, R. Hegerl, R. Guckenberger, M. Hahn, and W. O. Saxton.** 1986. Three-dimensional structure of the regular surface layer (HP1) layer of *Deinococcus radiodurans*. J. Mol. Biol. **187**:241–253.
3. **Baumeister, W., and H. Engelhardt.** 1987. Three-dimensional structure of bacterial surface layers, p. 109–154. *In* J. R. Harris and R. W. Horne (ed.), Electron microscopy of proteins, vol. 6. Academic Press, Inc. (London), Ltd., London.
4. **Baumeister, W., R. Guckenberger, H. Engelhardt, and C. L. F. Woodcock.** 1986. Metal shadowing and decoration in electron microscopy of biological macromolecules. Ann. N.Y. Acad. Sci. **483**:57–76.
5. **Bingle, W. H., J. L. Doran, and W. J. Page.** 1984. Regular surface layer of *Azotobacter vinelandii*. J. Bacteriol. **159**:251–259.
6. **Bingle, W. H., J. L. Doran, and W. J. Page.** 1986. Characterization of the surface layer protein from *Azotobacter vinelandii*. Can. J. Microbiol. **32**:112–120.
7. **Bingle, W. H., P. W. Whippey, J. L. Doran, R. G. E. Murray, and W. J. Page.** 1987. Structure of the *Azotobacter vinelandii* surface layer. J. Bacteriol. **169**:802–810.
8. **Buckmire, F. L. A., and R. G. E. Murray.** 1976. Substructure and in vitro reassembly of the outer, structured layer of *Spirillum serpens*. J. Bacteriol. **125**:290–299.
9. **Chalcroft, J. P., and C. L. Davey.** 1984. A simply constructed extreme-tilt holder for the Philips eucentric goniometer stage. J. Microsc. (Oxford) **134**:41–48.
10. **Chalcroft, J. P., H. Engelhardt, and W. Baumeister.** 1986. Three-dimensional structure of a regular surface layer from *Pseudomonas acidovorans*. Arch. Microbiol. **144**:196–200.
11. **DeWachter, R., E. Huysmans, and A. Vandenberghe.** 1985. 5S ribosomal RNA as a tool for studying evolution, p. 115–142. *In* K. H. Schleifer and E. Stackebrandt (ed.), Evolution of prokaryotes. Academic Press, Inc. (London) Ltd., London.
12. **Dickson, M. R., K. H. Downing, W. H. Wu, and R. M. Glaeser.** 1986. Three-dimensional structure of the surface layer protein of *Aquaspirillum serpens* VHA determined by electron crystallography. J. Bacteriol. **167**:1025–1034.
13. **Doran, J. L., W. H. Bingle, and W. J. Page.** 1987. Role of calcium in the assembly of the *Azotobacter vinelandii* surface array. J. Gen. Microbiol. **133**:399–413.
14. **Engelhardt, H., R. Guckenberger, R. Hegerl, and W. Baumeister.** 1985. High resolution shadowing of freeze-dried bacterial photosynthetic membranes: multivariate statistical analysis and surface relief reconstruction. Ultramicroscopy **16**:395–410.
15. **Engelhardt, H., W. O. Saxton, and W. Baumeister.** 1986. Three-dimensional structure of the tetragonal surface layer of *Sporosarcina ureae*. J. Bacteriol. **168**:309–317.
16. **Frank, J., and M. van Heel.** 1982. Correspondence analysis of aligned images of biological particles. J. Mol. Biol. **161**:134–137.
17. **Glauert, A. M., and M. J. Thornley.** 1973. Self-assembly of a surface component of a bacterial outer membrane. John Innes Symp. **1**:297–305.
18. **Guckenberger, R.** 1985. Surface reliefs derived from heavy-metal-shadowed specimens—Fourier space techniques applied to periodic objects. Ultramicroscopy **16**:357–370.
19. **Hastie, A. T., and C. C. Brinton.** 1979. Specific interaction of the tetragonally arrayed protein layer of *Bacillus sphaericus* with its peptidoglycan sacculus. J. Bacteriol. **138**:1010–1021.
20. **Hegerl, R., Z. Cejka, and W. Baumeister.** 1986. A bacterial S-layer: separation of double lattices, correlation averaging and 3-D reconstruction, p. 148–149. *In* G. W. Bailey (ed.), Proceedings of the 44th Annual Meeting of the Electron Microscopy Society of America. San Francisco Press, Inc., San Francisco.
21. **Houwink, A. L.** 1953. A macromolecular mono-layer in the cell wall of a *Spirillum* spec. Biochim. Biophys. Acta **10**:360.
22. **Koval, S. F., and R. G. E. Murray.** 1986. The superficial protein arrays on bacteria. Microbiol. Sci. **3**:357–361.
23. **Lepault, J., N. Martin, and K. Leonard.** 1986. Three-dimensional structure of the T-layer of *Bacillus sphaericus* P-1. J. Bacteriol. **168**:303–308.
24. **Robish, S. A., and A. G. Marr.** 1962. Localization of enzymes in *Azotobacter agilis*. J. Bacteriol. **83**:158–168.
25. **Saxton, W. O.** 1985. Computer generation of shaded images of solids and surfaces. Ultramicroscopy **16**:387–394.
26. **Saxton, W. O., and W. Baumeister.** 1982. The correlation averaging of a regularly arranged bacterial cell envelope protein. J. Microsc. (Oxford) **127**:127–138.
27. **Saxton, W. O., W. Baumeister, and M. Hahn.** 1984. Three-dimensional reconstruction of imperfect two-dimensional crystals. Ultramicroscopy **13**:57–70.
28. **Sleytr, U. B.** 1976. Self-assembly of the hexagonally and tetragonally arranged subunits of bacterial surface layers and their reattachment to cell walls. J. Ultrastruct. Res. **55**:360–377.
29. **Smit, J.** 1987. Protein surface layers of bacteria, p. 343–376. *In* M. Inouye (ed.), Bacterial outer membranes as model systems. John Wiley & Sons, New York.
30. **Stackebrandt, E., and C. R. Woese.** 1981. The evolution of prokaryotes. Symp. Soc. Gen. Microbiol. **32**:1–31.
31. **Stewart, M. J., T. J. Beveridge, and T. J. Trust.** 1986. Two patterns in the *Aeromonas salmonicida* A-layer may reflect a structural transformation that alters permeability. J. Bacteriol. **166**:120–127.